



## Combined spectral experiment and theoretical calculation to study the chemosensors of copper and their applications in anion bioimaging

Yutao Yang<sup>a,b,1</sup>, Fangjun Huo<sup>b,1</sup>, Caixia Yin<sup>a,\*</sup>, Yueyin Chu<sup>c</sup>, Jianbin Chao<sup>b</sup>, Yongbin Zhang<sup>b</sup>, Jingjing Zhang<sup>a</sup>, Sidian Li<sup>a</sup>, Haigang Lv<sup>a</sup>, Anmin Zheng<sup>c,\*\*</sup>, Diansheng Liu<sup>b,\*\*\*</sup>

<sup>a</sup> Key Laboratory of Chemical Biology and Molecular Engineering of Ministry of Education, Institute of Molecular Science, Shanxi University, Taiyuan 030006, China

<sup>b</sup> Research Institute of Applied Chemistry, Shanxi University, Taiyuan 030006, China

<sup>c</sup> Wuhan Center for Magnetic Resonance, State Key Laboratory of Magnetic Resonance and Atomic and Molecular Physics, Wuhan Institute of Physics and Mathematics, The Chinese Academy of Sciences, Wuhan 430071, China

### ARTICLE INFO

#### Article history:

Received 25 September 2012

Received in revised form 8 December 2012

Accepted 12 December 2012

Available online 21 December 2012

#### Keywords:

Chemosensors

Copper

UV-visible and fluorescence spectroscopy

DFT

Anion bioimaging

### ABSTRACT

Three salicylaldehyde derivatives, namely 5-nitrosalicylaldehyde fluorescein hydrazone (**1**), 5-diethylaminosalicylaldehyde fluorescein hydrazone (**2**), and di(5-diethylamino salicylaldehyde) hydrazide (**3**), were synthesized and characterized. Their ability to recognize copper ions was investigated by UV-visible and fluorescence spectroscopies, with **2** shown to be an optimal probe for effective detection of Cu<sup>2+</sup>. More importantly, to explore the optical properties of these probes, and their mechanism for recognition of Cu<sup>2+</sup> ions, B3LYP/6-311+G(d,p) density functional calculations were used to investigate the molecular orbitals and electronic excitations of each probe. In addition, because the **2**-Cu<sup>2+</sup> complex exhibits anion-induced fluorescence enhancement, we illustrate its potential application to bioimaging.

© 2012 Elsevier B.V. All rights reserved.

### 1. Introduction

Copper is among the more important of the transition metals in the human body and it is not only important for various physiological aspects, such as bone formation, cellular respiration, and connective tissue development, but also serves as an important catalytic cofactor for several metalloenzymes [1–4]. A deficiency of copper can lead to anemia or pancytopenia, whereas excess copper can lead to the mismetallation of other metal binding sites. Free copper acts as a catalyst for Fenton-type reactions, which produce reactive oxygen species, and misregulation of copper uptake is known to cause Menkes and Wilson's disease [5–7]. On the other hand, copper is the third most abundant essential trace element in the human body (after Fe<sup>2+</sup> and Zn<sup>2+</sup>) and is commonly found as Cu<sup>2+</sup> in natural water [8,9]. The recommended daily allowance of copper, as suggested by National Research Council ranges from 1.5 to 3.0 mg for adults, 1.5 to 2.5 mg for children, and 0.4 to 0.6 mg for infants [10]. According to the guidelines for drinking-water

quality of the World Health Organization, copper is identified as a “chemical of health significance in drinking-water” [11]. Copper is also a widely used industrial metal. Its cation is toxic at high concentrations [12], but in trace amounts it is also involved in brain diseases such as Alzheimer's and Parkinson's, and in prion disease [13,14]. Consequently, effective detection of Cu<sup>2+</sup> in water or physiological samples is of toxicological and environmental concern [15–18].

Copper ions can be detected using several instrumental techniques [19]. However, these methods are time-consuming and require expensive instrumentation. Chemosensors are powerful molecular tools that can be used to detect many different target molecules, including biological markers and environmental pollutants [20–25]. Many of these systems are based on well established and unique molecular frameworks, such as coumarins [26–28], quinolines [29], rhodamines [30–36], BOD-IPY dyes [37–39], calixarenes [40–43], and their detection process and mechanisms are also multifarious [26–46]. In our previous work, we studied and reported on two copper sensors [47,48]. In the present work, we report on the synthesis and characterization of three compounds that contain similar structures to each other: 5-nitrosalicylaldehyde fluorescein hydrazone (**1**), 5-diethylaminosalicylaldehyde fluorescein hydrazone (**2**), and di(5-diethylamino salicylaldehyde) hydrazide (**3**) (Fig. 1). We also investigated the recognition ability of these compounds to

\* Corresponding author. Tel.: +86 351 7011022; fax: +86 351 7011022.

\*\* Corresponding author. Tel.: +86 27 87199291; fax: +86 27 87199291.

\*\*\* Corresponding author.

E-mail addresses: [yincx@sxu.edu.cn](mailto:yincx@sxu.edu.cn) (C. Yin), [zhenganm@wipm.ac.cn](mailto:zhenganm@wipm.ac.cn) (A. Zheng).

<sup>1</sup> These authors contributed equally to this work.

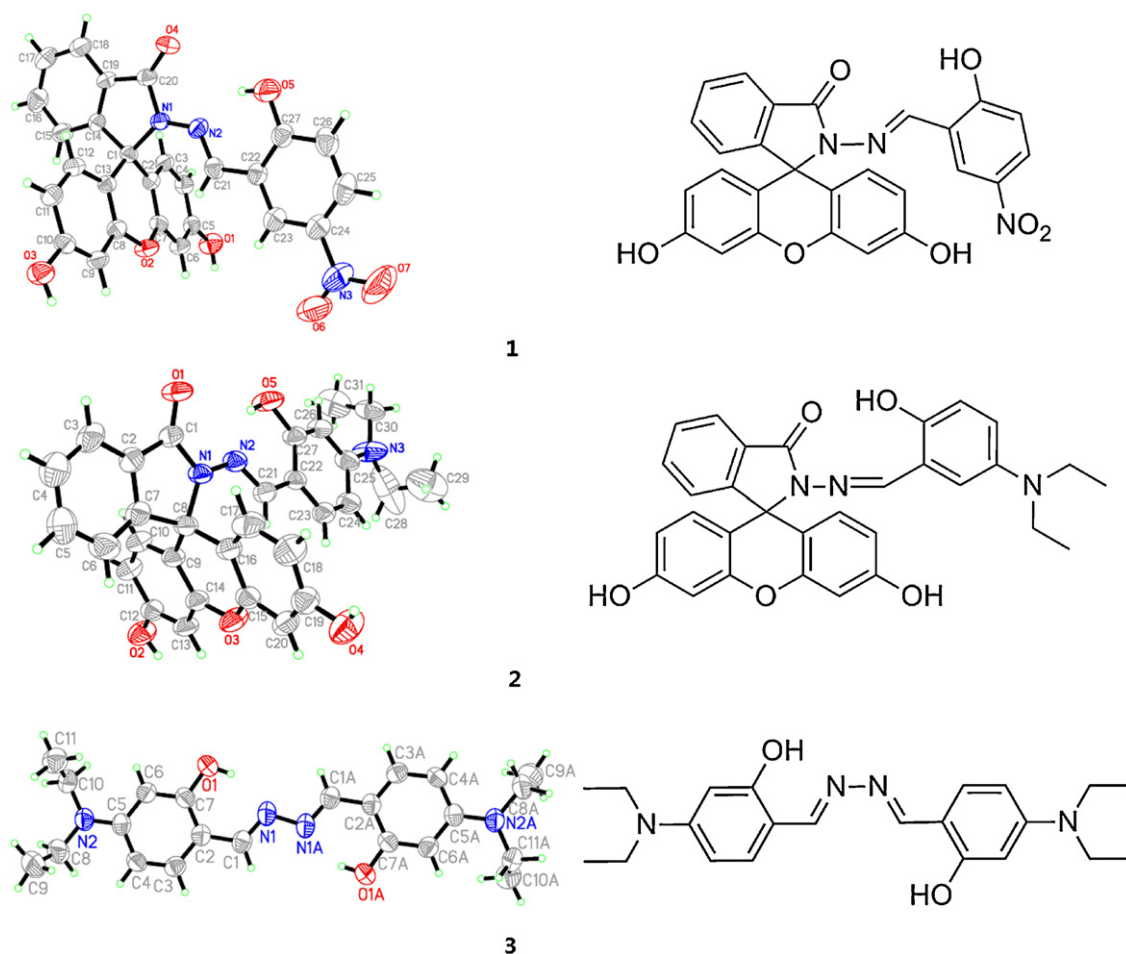


Fig. 1. The structure (top) and thermal ellipsoids of probes are drawn at the 50% probability level.

recognize copper using UV–visible (UV–vis) and fluorescence spectroscopies. Moreover, combinations of the electrospray ionization mass spectrometry (ESI–MS) and theoretical calculation were used to clarify the recognition process involved with these species. On the basis of our studies, it is demonstrated that, as probes for copper, there are significant differences in ability between these three compounds, despite their similar structure. For example, **1** as a UV–vis probe shows markedly different results from the other probes tested, both in terms of UV–vis and fluorescence probes. Both **2** and **3** act as fluorescence on–off probes; however, one distinguishing feature of **3** is that when it is in the *anti* configuration, upon meeting with  $\text{Cu}^{2+}$  it first transforms into the *syn* configuration and then coordinates with  $\text{Cu}^{2+}$ , consequently resulting in fluorescence quenching. In addition, bioimaging was carried out with the **2**– $\text{Cu}^{2+}$  complex because it exhibits anion-induced fluorescence enhancement with a selection of anions.

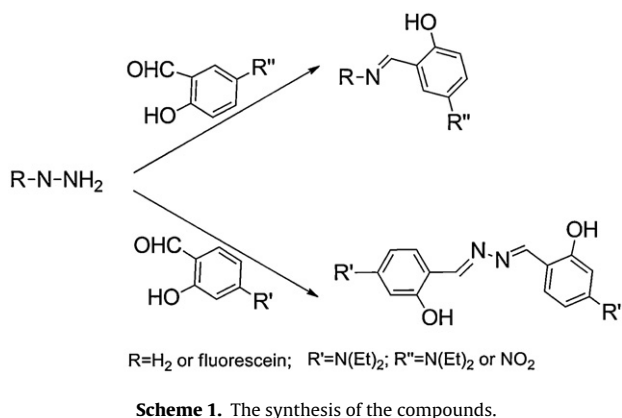
## 2. Materials and methods

### 2.1. Materials

4-(2-Hydroxyethyl)-1-piperazineethanesulfonic acid (HEPES) was purchased from Sigma–Aldrich (St. Louis, MO). Sodium hydroxide solution (0.1 mol/L) was added to aqueous HEPES (10 mmol/L) to adjust the pH to 7.0. Cationic salts were purchased from Shanghai Experiment Reagent Co., Ltd., China. All other chemicals used were of analytical grade.

### 2.2. Instruments

A pH meter (Mettler Toledo, Switzerland) was used to determine the pH. Ultraviolet–visible (UV–vis) spectra were recorded on a Cary 50 Bio UV–Vis spectrophotometer. Fluorescence spectra were measured on Cary Eclipse fluorescence spectrophotometer. A PO-120 quartz cuvette (10 mm) was purchased from Shanghai Huamei Experiment Instrument Plants, China.  $^1\text{H}$  NMR,  $^{13}\text{C}$  NMR spectra were recorded on a Bruker AVANCE-300 MHz and 75 MHz NMR spectrometer, respectively (Bruker, Billerica, MA). Electron bombard ionization mass spectrometry (EI–MS) was measured with GCT–MS (Waters) instrument. ESI was measured with an LTQ–MS (Thermo) instrument. The ability of **2**– $\text{Cu}^{2+}$  reacting to anion in the living cells was also evaluated by laser confocal fluorescence imaging using an Leica TCS SP5 laser scanning microscope. The yellow single crystals of **1**, **2**, and **3** were mounted on a glass fiber for data collection. Cell constants and an orientation matrix for data collection were obtained by least-squares refinement of diffraction data from reflections within  $1.00\text{--}25.05^\circ$ ,  $1.00\text{--}25.05^\circ$ , and  $0.99\text{--}27.46^\circ$ , using a Bruker SMART APEX CCD automatic diffractometer. Data were collected at 296 K using Mo  $\text{K}\alpha$  radiation ( $\lambda = 0.710713 \text{ \AA}$ ) and the  $\omega$ -scan technique, and corrected for the Lorentz and polarization effects (SADABS) [49]. The structures were solved by direct methods (SHELX97) [50], and subsequent difference Fourier maps were inspected and then refined in F2 using a full-matrix least-squares procedure and anisotropic displacement parameters.



### 2.3. Preparation of 1, 2, and 3

The synthesis of compounds **1**, **2**, and **3** are summarized in Scheme 1. **1** and **2** were synthesized by a one-step reaction between fluorescein hydrazine and either of 5-nitrosalicylaldehyde (for **1**), 5-diethylaminosalicylaldehyde (for **2**) in methanol containing acetic acid. 0.167 g (1 mmol) 5-nitrosalicylaldehyde (for **1**) or 0.193 g (1 mmol) 5-diethylaminosalicylaldehyde (for **2**) were added to 0.35 g (1 mmol) of fluorescein hydrazine dissolved in 20 ml of methanol and the reaction solution refluxed in an oil bath for 2 h. A white solid appeared which was then filtered from each solution. Each crude product was recrystallized in CH<sub>3</sub>OH and petroleum ether (v/v, 1/1) to give 5-nitrosalicylaldehyde fluorescein hydrazone (**1**) or 5-diethylaminosalicylaldehyde fluorescein hydrazone (**2**) as a yellow powder in 60%, and 65% yields, respectively (Fig. S1). An H<sub>2</sub>O/CH<sub>3</sub>CH<sub>2</sub>OH solution containing the product was allowed to evaporate slowly at room temperature for several days, and the yellow crystals that subsequently formed were suitable for X-ray crystallography formed. **1**: mp 385 °C; FT-IR (KBr, cm<sup>-1</sup>): 3388 (–OH), 3092 (Ar–H), 1696 (C=O), 1630 (C=N), 1262 (C–O); <sup>1</sup>H NMR (300 MHz, 25 °C, DMSO-*d*<sub>6</sub>): δ 11.61 (s, 1H), 9.92 (bs, 2H), 9.05 (s, N=C–H, 1H), 8.30 (d, 1H), 8.06 (d, 1H, *J* = 9.1 Hz), 7.94 (m, 1H, *J* = 6.7 Hz), 7.64 (t, 2H, *J* = 7.2 Hz), 7.13 (d, 1H, *J* = 6.8 Hz), 6.95 (d, 1H, *J* = 9.0 Hz), 6.66 (bs, 2H), 6.49 (d, 4H, *J* = 9.9 Hz); <sup>13</sup>C NMR (75 MHz, DMSO-*d*<sub>6</sub>): δ 171.48, 169.85, 166.40, 159.80, 158.33, 151.62, 147.63, 142.04, 136.89, 135.57, 134.45, 131.48, 131.20, 130.20, 128.21, 126.55, 124.64, 120.20, 117.09, 110.26, 72.88; EI-MS *m/z* 495 [1]<sup>+</sup>; Elemental analysis (calcd. %) for C<sub>27</sub>H<sub>17</sub>N<sub>3</sub>O<sub>7</sub>: C, 65.45; H, 3.46; N, 8.48; Found: C, 65.48; H, 3.44, N, 8.54; Crystal data for C<sub>27</sub>H<sub>17</sub>N<sub>3</sub>O<sub>7</sub>: crystal size: 0.30 × 0.20 × 0.20, monoclinic, space group P2<sub>1</sub>/n (No. 11). *a* = 11.393(2) Å, *b* = 15.307(3) Å, *c* = 14.354(3) Å, β = 112.338°, *V* = 2315.4(8) Å<sup>3</sup>, *Z* = 4, *T* = 296 K, θ<sub>max</sub> = 25.05°, 12,799 reflections measured, 4097 unique (*R*<sub>int</sub> = 0.0707). Final residual for 338 parameters and 4097 reflections with *I* > 2σ(*I*): *R*<sub>1</sub> = 0.0500, *wR*<sub>2</sub> = 0.0677 and GOF = 1.265 (Fig. S2).

**2**: mp 325 °C; FT-IR (KBr, cm<sup>-1</sup>): 3317 (–OH), 3072 (Ar–H), 2971 (C–H, CH<sub>3</sub>), 2930 (C–H, CH<sub>2</sub>), 1696 (C=O), 1632 (C=N), 1262 (C–O); <sup>1</sup>H NMR (300 MHz, 25 °C, DMSO-*d*<sub>6</sub>): δ 10.38 (s, 1H), 9.87 (bs, 2H), 8.95 (s, N=C–H, 1H), 7.83 (d, 1H), 7.56 (d, 2H), 7.08 (m, 1H), 6.97 (t, 1H, *J* = 8.3 Hz), 6.58 (d, 2H), 6.43 (d, 4H, *J* = 8.2 Hz), 6.13 (bs, 1H), 5.91 (d, 1H), 2.04 (m, 4H), 0.99 (m, 6H); <sup>13</sup>C NMR (75 MHz, DMSO-*d*<sub>6</sub>): δ 159.30, 158.20, 154.43, 151.84, 150.12, 149.66, 133.22, 131.69, 129.14, 128.73, 127.81, 123.38, 122.54, 112.06, 109.23, 105.87, 103.44, 102.03, 96.93, 64.87, 43.44, 12.06; EI-MS *m/z* 521 [2]<sup>+</sup>; Elemental analysis (calcd. %) for C<sub>31</sub>H<sub>27</sub>N<sub>3</sub>O<sub>5</sub>: C, 71.39; H, 5.22; N, 8.06; Found: C, 71.38; H, 5.25, N, 8.04; Crystal data for C<sub>35</sub>H<sub>31</sub>N<sub>5</sub>O<sub>5</sub>: crystal size: 0.30 × 0.20 × 0.20, monoclinic, space group P2<sub>1</sub>/c (No. 14). *a* = 18.555(7) Å, *b* = 10.094(4) Å, *c* = 17.258(7) Å, β = 97.832(7)°, *V* = 3202(2) Å<sup>3</sup>, *Z* = 4, *T* = 296 K, θ<sub>max</sub> = 25.05°, 33,239 reflections

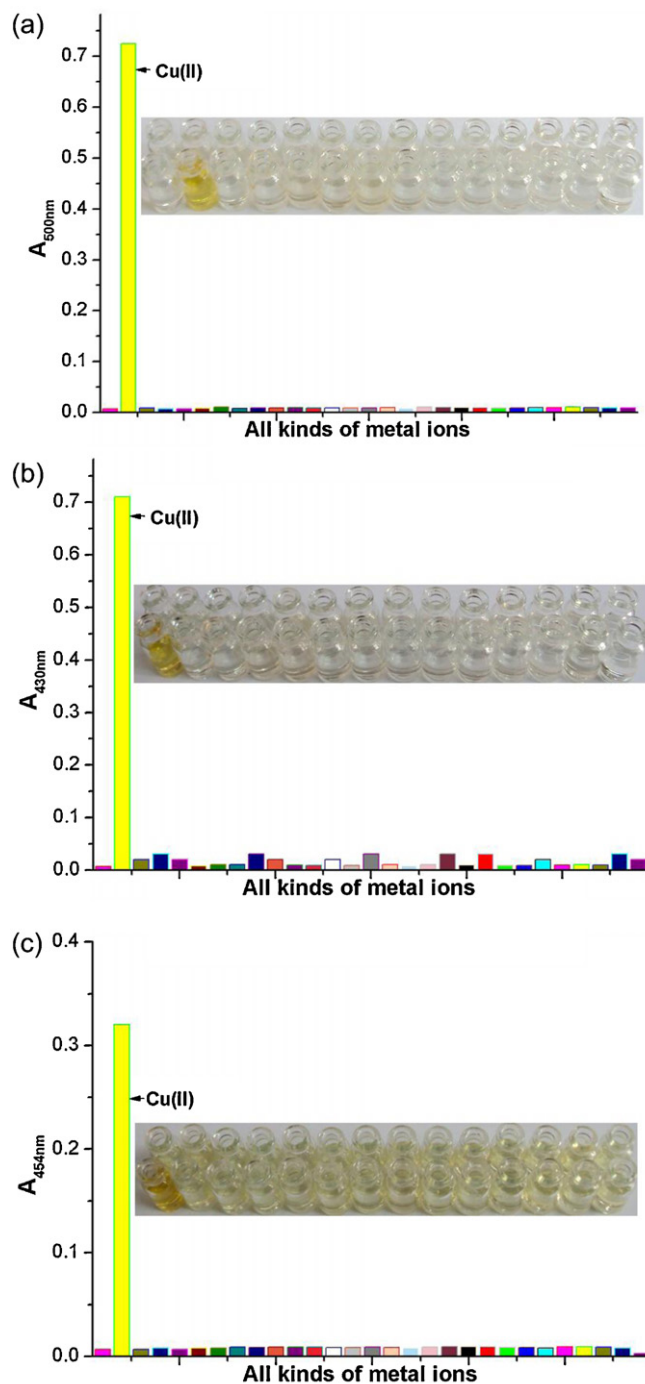


**Fig. 2.** Optical density two-dimensional graph of the three probes (a), (b), and (c) at 500 nm (**1**), 430 nm (**2**), 454 nm (**3**), respectively upon the addition of several metal ions (including Cu<sup>2+</sup>, Cu<sup>+</sup>, Ca<sup>2+</sup>, Fe<sup>2+</sup>, Zn<sup>2+</sup>, Ni<sup>2+</sup>, Bi<sup>3+</sup>, Co<sup>2+</sup>, VO<sup>2+</sup>, Mn<sup>2+</sup>, Ru<sup>3+</sup>, Cd<sup>2+</sup>, Pb<sup>2+</sup>, Ag<sup>+</sup>, La<sup>3+</sup>, Ce<sup>4+</sup>, Yb<sup>3+</sup>, Cr<sup>2+</sup>, Er<sup>3+</sup>, Mg<sup>2+</sup>, Sn<sup>2+</sup>, Al<sup>3+</sup>, Nd<sup>3+</sup>, Zr<sup>4+</sup>, K<sup>+</sup>, Sm<sup>3+</sup>, Fe<sup>3+</sup>, Eu<sup>3+</sup>). Inset: a color change photograph for Cu<sup>2+</sup> and the other metal ions. (For interpretation of the references to color in this figure legend, the reader is referred to the web version of the article.)

measured, 5662 unique (*R*<sub>int</sub> = 0.0904). Final residual for 365 parameters and 5662 reflections with *I* > 2σ(*I*): *R*<sub>1</sub> = 0.0899, *wR*<sub>2</sub> = 0.2902 and GOF = 1.029 (Fig. S3).

**3** was synthesized by a one-step reaction of 5-diethylaminosalicylaldehyde with excess hydrazine hydrate in ethanol, in accordance with the procedure reported in the literature [51]. An excessive hydrazine hydrate (85%, 1.2 mL) was added

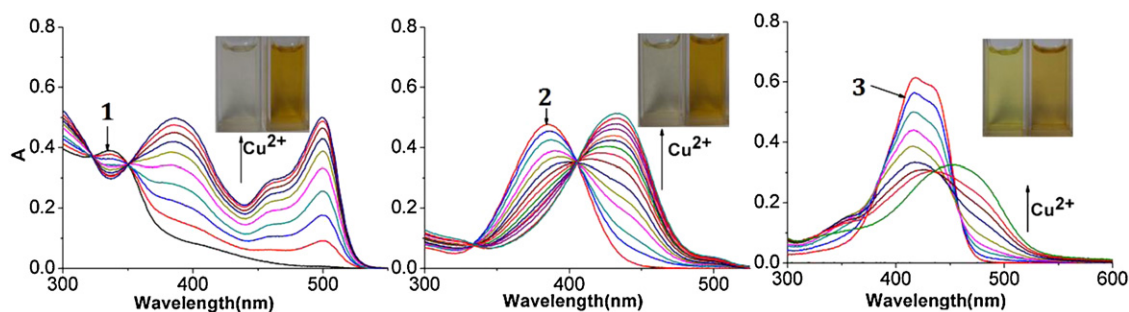


**Fig. 3.** Absorption spectral changes of three probes in 10 mM HEPES at pH 7.0 as an aqueous buffer upon the addition of  $\text{Cu}^{2+}$ ;  $\text{Cu}^{2+}$  was added gradually with  $[\text{Cu}^{2+}] = 0\text{--}25$ ,  $0\text{--}16$ , and  $0\text{--}9$   $\mu\text{M}$ , respectively; each spectrum was recorded 30 s after  $\text{Cu}^{2+}$  addition. Inset: a color change photograph for  $\text{Cu}^{2+}$  and three probes. (For interpretation of the references to color in this figure legend, the reader is referred to the web version of the article.)

to a 0.193 g (1 mmol) of di(5-diethylamino salicylaldehyde) that had been dissolved in 20 ml of ethanol. The reaction solution was then refluxed in an oil bath for 8 h and a brown oily product was obtained by evacuating the ethanol under reduced pressure. The solid product was precipitated by adding water and recrystallized from ethanol–water to give di(5-diethylamino salicylaldehyde) hydrazide (**3**) as yellow powder in 80% yield (0.15 g) (Fig. S1). An  $\text{H}_2\text{O}/\text{CH}_3\text{CH}_2\text{OH}$  solution of **3** was allowed to evaporate slowly at room temperature for several days and yellow crystals that were formed were suitable for X-ray crystallography. mp 219–221 °C; FT-IR (KBr,  $\text{cm}^{-1}$ ): 3404 (–OH), 3080 (Ar–H), 2971 (C–H,  $\text{CH}_3$ ), 2930 (C–H,  $\text{CH}_2$ ), 1585 (C=C), 1630 (C=N);  $^1\text{H}$  NMR (300 MHz,  $25^\circ\text{C}$ ,  $\text{DMSO}-d_6$ ):  $\delta$  11.48 (bs, 2H), 8.61 (bs, N=C–H, 2H), 7.28 (d, Ar–H, 2H,  $J=8.7$  Hz), 6.30 (t, Ar–H, 2H,  $J=9.7$  Hz), 6.11 (s, t, 2H), 2.08 (m,  $\text{CH}_2\text{--H}$ , 8H,  $J=6.9$  Hz), 1.10 (t,  $\text{CH}_3\text{--H}$ , 12H,  $J=6.5$  Hz);  $^{13}\text{C}$  NMR (75 MHz,  $\text{DMSO}-d_6$ ):  $\delta$  160.34, 150.58, 132.72, 106.06, 103.71, 96.70, 43.55, 38.34, 30.39, 12.23; EI-MS  $m/z$  382 [**3**] $^+$ ; Elemental analysis (calcd. %) for  $\text{C}_{22}\text{H}_{30}\text{N}_4\text{O}_2$ : C, 69.08; H, 7.91; N, 14.65; Found: C, 69.11; H, 7.94; N, 14.64; Crystal data for  $\text{C}_{22}\text{H}_{30}\text{N}_4\text{O}_2$ : crystal size:  $0.21 \times 0.18 \times 0.16$ , monoclinic, space group  $\text{P}2(1)/n$  (No. 11).  $a = 11.722(2)$  Å,  $b = 6.5173(13)$  Å,  $c = 13.320(3)$  Å,  $\beta = 96.42^\circ$ ,  $V = 1011.2(3)$  Å $^3$ ,  $Z = 2$ ,  $T = 173$  K,  $\theta_{\text{max}} = 27.46^\circ$ , 4981 reflections measured, 2314 unique ( $R_{\text{int}} = 0.0390$ ). Final residual for 129 parameters and 2314 reflections with  $I > 2\sigma(I)$ :  $R_1 = 0.0589$ ,  $wR_2 = 0.1427$  and  $\text{GOF} = 1.047$  (Fig. S4).

#### 2.4. UV–vis and fluorescence spectroscopies

A  $\text{Cu}^{2+}$  solution was prepared by dissolving copper chloride in deionized water. Probes stock solutions were prepared in ethanol. UV–vis and fluorescence spectra were obtained in 2-[4-(2-hydroxyethyl)-1-piperazinyl]ethanesulfonic acid, HEPES aqueous buffer (10 mmol/L, pH 7.0) solutions. Aqueous anion solutions were

also prepared using deionized water. Fluorescence measurements were carried out with a slit width of 5 nm.

#### 2.5. Computational methods

All calculations reported in this work were performed using Gaussian 09 suite of programs. Ground-state geometries and electron structures of the complexes were optimized by means of the density functional theory (DFT) using the B3LYP/6-311++G (d,p) basis set. Time-dependent DFT (TD-DFT) calculations were used to determine optical properties of the complexes based on their optimized ground-state geometries. Geometrical optimization for the  $\text{Cu}^{2+}$ -addition products were performed using the UB3LYP functional combined with the 6-311+G(d,p) basic set for C, H, N and F atoms and the LANL2DZ basis set for the Cu atoms.

### 3. Results and discussion

#### 3.1. Selectivity over metal ions

The effect of a wide range of environmentally and physiologically active metal ions was investigated for each of compounds **1**, **2**, and **3** using the UV–vis spectra of solutions containing these compounds and the metal ion (100 equiv.) in HEPES aqueous buffer (10 mmol/L, pH 7.0). The results showed that whereas metal ions such as  $\text{Cu}^+$  (sodium ascorbate as stabilizer),  $\text{Ca}^{2+}$ ,  $\text{Fe}^{2+}$ ,  $\text{Zn}^{2+}$ ,  $\text{Ni}^{2+}$ ,  $\text{Bi}^{3+}$ ,  $\text{Co}^{2+}$ ,  $\text{VO}^{2+}$ ,  $\text{Mn}^{2+}$ ,  $\text{Ru}^{3+}$ ,  $\text{Cd}^{2+}$ ,  $\text{Pb}^{2+}$ ,  $\text{Ag}^+$ ,  $\text{La}^{3+}$ ,  $\text{Ce}^{4+}$ ,  $\text{Yb}^{3+}$ ,  $\text{Cr}^{2+}$ ,  $\text{Er}^{3+}$ ,  $\text{Mg}^{2+}$ ,  $\text{Sn}^{2+}$ ,  $\text{Al}^{3+}$ ,  $\text{Nd}^{3+}$ ,  $\text{Zr}^{4+}$ ,  $\text{K}^+$ ,  $\text{Sm}^{3+}$ ,  $\text{Fe}^{3+}$  and  $\text{Eu}^{3+}$  do not result in any apparent changes in absorption peaks, there is notable change when  $\text{Cu}^{2+}$  is involved. Fig. 2 shows that when  $\text{Cu}^{2+}$  is added, strong new absorption peaks appear at 500, 430, or 454 nm for probe **1**, **2**, or **3**, respectively. We also note that the color of the solution changes from a light yellow to an orange yellow.

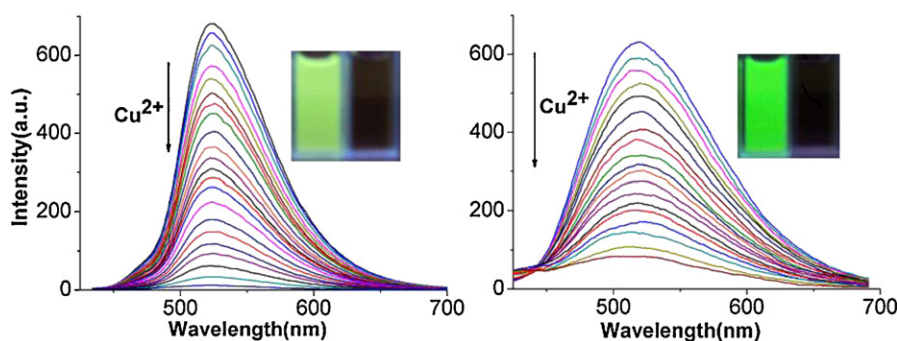


**Fig. 4.** Fluorescence spectral changes for **2** and **3** probes upon the addition of  $\text{Cu}^{2+}$  in 10 mM HEPES at pH 7.0 as an aqueous buffer with  $[\text{Cu}^{2+}] = 0\text{--}0.18$  and  $0\text{--}0.5$   $\mu\text{M}$ , respectively. Inset: color (left) and visual fluorescence (right) change photographs for probes upon the addition of  $\text{Cu}^{2+}$  in a HEPES (pH 7.0) buffer solution under UV illumination (365 nm). (For interpretation of the references to color in this figure legend, the reader is referred to the web version of the article.)

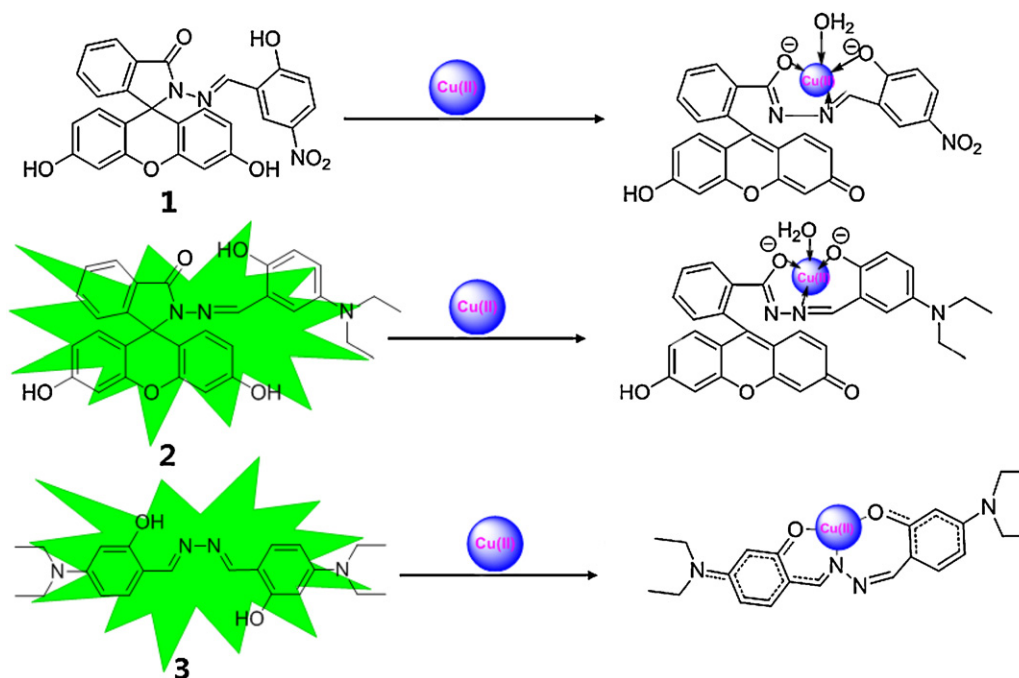


Fig. 5. The proposed structures organized by the  $\text{Cu}^{2+}$  ion when it coordinates with probes to form complexes.

### 3.2. UV–vis spectra of detecting $\text{Cu}^{2+}$

A detailed investigation was carried out into the ability of the three compounds to recognize  $\text{Cu}^{2+}$ . Fig. 3 (left) shows that a regular change in the UV–visible spectrum can be observed when the  $\text{Cu}^{2+}$  solution is added to the HEPES buffer (10 mM, pH 7.0) containing **1** (25  $\mu\text{mol/L}$ ). With an increase in the  $\text{Cu}^{2+}$  concentration, new absorption peaks appear at 386 and 500 nm, and  $A_{386,500\text{nm}}$  gradually increases with isosbestic point at 322 and 350 nm, indicating that there has been formation of a new complex. From the concentration of  $\text{Cu}^{2+}$ , the stoichiometric relationship between the probe and  $\text{Cu}^{2+}$  was found to be 1:1 based on the change in absorbance at 500 nm. Fig. 3 (middle) shows that there is a change in the UV–visible spectrum when the  $\text{Cu}^{2+}$  solution is added to the HEPES buffer (10 mmol/L, pH 7.0) containing **2** (16  $\mu\text{mol/L}$ ). With an increase in the  $\text{Cu}^{2+}$  concentration, a new absorption peak appears at 430 nm and  $A_{430\text{nm}}$  gradually increases with an isosbestic point formed at 404 nm. The stoichiometric relationship between the probe and  $\text{Cu}^{2+}$  was found to be 1:1 based on the change in absorbance at 430 nm. Fig. 3 (right) shows the UV–vis spectra obtained when the solution of  $\text{Cu}^{2+}$  was titrated into the buffer of **3** (9  $\mu\text{mol/L}$ ). Upon the addition of  $\text{Cu}^{2+}$ , the maximum absorption peak gradually shifted from light yellow ( $\lambda_{\text{max}} = 418\text{ nm}$ ) to orange yellow ( $\lambda_{\text{max}} = 454\text{ nm}$ ). The stoichiometric relationship between the probe and  $\text{Cu}^{2+}$  was found to be 1:1. We also studied the ability of each compound to detect  $\text{Cu}^{2+}$  in the presence of several metal ions. Fig. S5 shows that the other ions did not interfere with the determination of  $\text{Cu}^{2+}$ .

### 3.3. pH dependence

The pH range for the determination of  $\text{Cu}^{2+}$  was also studied. For probe **1**, no absorption peak at 500 nm was induced by  $\text{Cu}^{2+}$  when the solution pH was between 2 and 6. However, probe **1** shows a good response to  $\text{Cu}^{2+}$  in the pH range pH 7–12. Therefore, physiological acidity (pH 7.0) was selected for further investigation. Free probe **2** shows absorption at 500 nm for pH 12 and 13, and it also has no fluorescent emission when pH value is 2, 12, or 13. Similar to **1**, probe **2** illustrates a good response to  $\text{Cu}^{2+}$  in the pH range

7–10, with the result that pH 7.0 was also selected for further study with this probe. Using free probe **3**, the absorption peak shifts when the pH is 3, 4, 12, or 13 and there is fluorescence quenching at pH 2, 3, 12, or 13. When the solution pH is 3, 5, or 6,  $\text{Cu}^{2+}$  induced a fluorescence intensity for probe **3** such that there was either no quenching or only partial quenching. Therefore, the pH range of 7–10 is effective for this probe and neutral pH was used for further studies (Fig. S6).

### 3.4. Time-dependence in the detection process of $\text{Cu}^{2+}$

Time-dependent variations in the UV–vis of **1**, **2**, and **3** were monitored in the presence of 10 equiv. of  $\text{Cu}^{2+}$ . The kinetic study showed that the reaction was complete within 15, 5, and 3 s for  $\text{Cu}^{2+}$  with **1**, **2**, and **3**, respectively, thus indicating that these probes react very rapidly with  $\text{Cu}^{2+}$  under the experimental conditions considered (Fig. S7).

### 3.5. Fluorescence spectra

The fluorescence spectra of each of the probes with an increased concentration of  $\text{Cu}^{2+}$  in HEPES buffer are displayed in Fig. 4. The addition of  $\text{Cu}^{2+}$  resulted in no variation to the fluorescence spectra of **1**. However, the addition of  $\text{Cu}^{2+}$  did lead to fluorescence quenching for remaining two probes (**2**:  $\lambda_{\text{ex}} = 382\text{ nm}$  and  $\lambda_{\text{em}} = 520\text{ nm}$ ; **3**:  $\lambda_{\text{ex}} = 425\text{ nm}$  and  $\lambda_{\text{em}} = 524\text{ nm}$ ). Fig. S8 shows the fluorescence changes that the probes undergo upon the addition of various metal ions, including  $\text{Cu}^+$  (sodium ascorbate as stabilizer),  $\text{Ca}^{2+}$ ,  $\text{Fe}^{2+}$ ,  $\text{Zn}^{2+}$ ,  $\text{Ni}^{2+}$ ,  $\text{Bi}^{3+}$ ,  $\text{Co}^{2+}$ ,  $\text{VO}^{2+}$ ,  $\text{Mn}^{2+}$ ,  $\text{Ru}^{3+}$ ,  $\text{Cd}^{2+}$ ,  $\text{Pb}^{2+}$ ,  $\text{Ag}^+$ ,  $\text{La}^{3+}$ ,  $\text{Ce}^{4+}$ ,  $\text{Yb}^{3+}$ ,  $\text{Cr}^{2+}$ ,  $\text{Er}^{3+}$ ,  $\text{Mg}^{2+}$ ,  $\text{Sn}^{2+}$ ,  $\text{Al}^{3+}$ ,  $\text{Nd}^{3+}$ ,  $\text{Zr}^{4+}$ ,  $\text{K}^+$ ,  $\text{Sm}^{3+}$ ,  $\text{Fe}^{3+}$  and  $\text{Eu}^{3+}$  in HEPES (10 mmol/L, pH 7.0). Unlike with  $\text{Cu}^{2+}$ , these other metal ions listed induced no change to the fluorescence emission properties under the same conditions besides.

### 3.6. Proposed mechanism

The proposed mechanisms of detection and the structures of the probes, both with and without the addition of  $\text{Cu}^{2+}$ , are shown in Fig. 5. Probe **1**, which exhibits strong intramolecular charge transfer

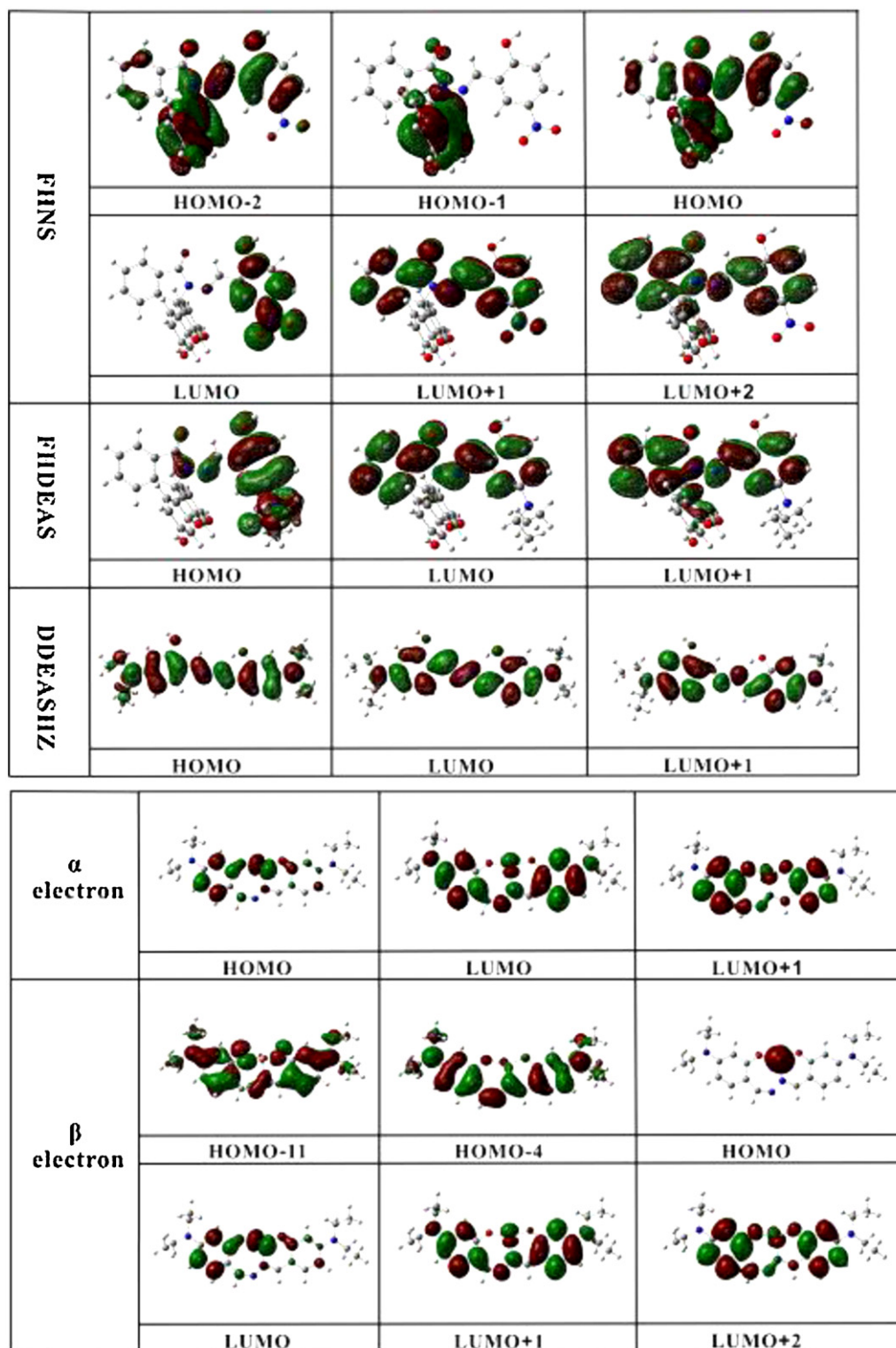


Fig. 6. (a) Molecular surfaces of the three probes; (b) molecular surfaces of DDEASHZ-Cu.

(ICT), is itself nonfluorescent, and the  $1\text{-Cu}^{2+}$  adduct remains non-fluorescent because of the paramagnetism effect from spin-orbit coupling of the  $\text{Cu}^{2+}$  (Fig. S9). Mass spectrometry analysis of a product obtained from the reaction of **1** with  $\text{Cu}^{2+}$  in  $\text{CH}_3\text{OH}$  shows binding between **1** and  $\text{Cu}^{2+}$ , a peak at  $m/z=574.08$ , corresponding to  $[1\text{-Cu}^{2+}\text{-H}_2\text{O}+\text{H}]^+$ , is clearly observed (see Fig. S10). Probe **2** exhibits strong fluorescence in its natural form. However, though the ring is open after coordination with  $\text{Cu}^{2+}$ , the

paramagnetic effect from spin-orbit coupling of the  $\text{Cu}^{2+}$  induces fluorescence quenching (Fig. S11). A peak at  $m/z=623.11$  corresponds to  $[2\text{-Cu(II)-H}_2\text{O}+\text{Na}]^+$  (Fig. S12). The complexes discussed above involving the ligands and copper ion are similar to forms reported previously [52–56]. Free probe **3** is in the *anti* configuration but upon encountering the  $\text{Cu}^{2+}$  it first transforms into the *syn* configuration before coordinating to the  $\text{Cu}^{2+}$ , resulting in fluorescence quenching (Fig. S13). From ESI-MS, a peak at  $m/z=466.14$

**Table 1**  
Calculated TD-DFT excitation properties and experimental  $\lambda$ .

	$\lambda$ (nm) (eV)		Dominant excitations
	Theory	Exp	
FHNS	333	334	H-1 $\rightarrow$ L+1 (0.48822) H-2 $\rightarrow$ L (0.33313) H $\rightarrow$ L+1 (0.31531)
FHNS-Cu	381	386	H-2 $\alpha$ $\rightarrow$ L $\alpha$ (0.52149) H-2 $\beta$ $\rightarrow$ L $\beta$ (0.36026) H-2 $\beta$ $\rightarrow$ L+1 $\beta$ (0.53653)
	503	500	H-2 $\alpha$ $\rightarrow$ L $\alpha$ (0.64491) H-2 $\beta$ $\rightarrow$ L+1 $\beta$ (0.66885)
FHDEAS	392	384	H $\rightarrow$ L (0.70017)
FHDEAS-Cu	424	432	H $\alpha$ $\rightarrow$ L+1 $\alpha$ (0.34363) H-2 $\beta$ $\rightarrow$ L+1 $\beta$ (0.33687) H $\beta$ $\rightarrow$ L+2 $\beta$ (0.42211)
	401	417	H $\rightarrow$ L (0.70317)
DDEASHZ-Cu	444	457	H $\alpha$ $\rightarrow$ L $\alpha$ (0.45366) H-11 $\beta$ $\rightarrow$ L $\beta$ (0.38095) H-4 $\beta$ $\rightarrow$ L $\beta$ (0.41407) H $\beta$ $\rightarrow$ L+1 $\beta$ (0.46609)

H and L denote the HOMO and LUMO, respectively and data in parentheses are coefficient of the wave function for each excitation. And  $\alpha$  and  $\beta$  denote  $\alpha$  and  $\beta$  electrons orbital of the Cu<sup>2+</sup>-products.

clarified the structure that results from coordination between **3** and Cu<sup>2+</sup> (Fig. S14), where the Cu<sup>2+</sup> is coordinated by N and O atoms of **3** [57].

### 3.7. Theoretical predictions

Theoretical calculations were explored to further study the optical properties of the probes and their Cu<sup>2+</sup>-addition products. As shown in Table 1, the TD-DFT calculations reveal that the main adsorption peaks for the three probes are 333 nm (**1**), 392 nm (**2**), and 401 nm (**3**), in close agreement with the experimentally observed adsorption spectra (as shown in Fig. 3). The main absorption bands in **2** (392 nm) and **3** (401 nm) originate from the highest occupied molecular orbital (HOMO)  $\rightarrow$  the lowest unoccupied molecular orbital LUMO transitions. However, the 333 nm

adsorption peak of **1** originates from (HOMO-1)  $\rightarrow$  (LUMO+1), (HOMO-2)  $\rightarrow$  LUMO, and HOMO  $\rightarrow$  (LUMO+1) mono-electronic excitations (see Table 1). On the basis of the molecular orbitals (Fig. 6), the electron density can be said to be mainly located on the same part of the HOMO and LUMO for **2** and **3**, but on different parts of the HOMO and LUMO for **1**. Such different characteristics of the calculated molecular orbitals demonstrate that **1** possesses a stronger ICT than **2** and **3**. It is well known that the fluorogenic process can be facilitated by the ICT mechanism [58–60]. Therefore, the different ICT processes in evidence for the three probes result in strong fluorescence emissions for **2** and **3** and weaker fluorescence emission for **1**, in accordance with the results determined herein by our experiment.

For the Cu<sup>2+</sup>-addition products of the three probes, the adsorption peak predicted by the theoretical methods is red-shifted compared with those of the independent probes (Table 1), which is in good agreement with the experimental observations. For example, upon the addition of Cu<sup>2+</sup> to **3**, the maximum absorption peak was gradually shifted from 401 nm to 444 nm. Based on the calculated molecular orbitals (Fig. 6), the conjugated system is broken with the Cu-products and this change will lead to a strong ICT process in the Cu-product. This can therefore explain the fluorescence quenching of the Cu-addition products that is witnessed experimentally.

### 3.8. Detection range

To investigate the detection limit of the probes for Cu<sup>2+</sup>, **1** (25  $\mu$ mol/L) was treated with various concentrations of Cu<sup>2+</sup> (0–25  $\mu$ mol/L) and the absorbance intensity at 500 nm was plotted as a function of Cu<sup>2+</sup> concentration (Fig. S15). The absorbance intensity of **1** is linearly proportional to the Cu<sup>2+</sup> concentration, and a concentration of Cu<sup>2+</sup> as low as 1.89  $\mu$ mol/L can be detected using **1**. In a similar procedure, **2** (0.1875  $\mu$ mol/L) was treated with various concentrations of Cu<sup>2+</sup> (0–9.375  $\mu$ mol/L) and the emission intensity at 520 nm plotted as a function of the Cu<sup>2+</sup> concentration. From this it can be seen that a concentration of Cu<sup>2+</sup> as low as 0.11  $\mu$ mol/L can be detected using **2**. Similarly, the detection limit was estimated to be less than 0.011  $\mu$ mol/L for **3**. These detection limits indicate that fluorescence probes **2** and **3** show a high

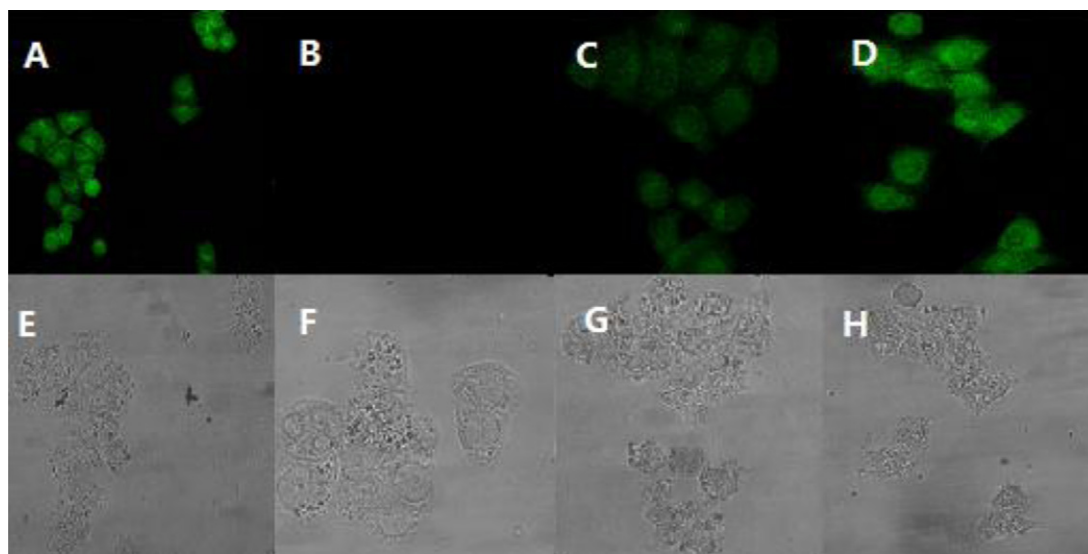


**Fig. 7.** Confocal fluorescence images in HepG2 cells. (A) Fluorescence image of HepG2 cells with adding **2** (10  $\mu$ M). (B) Fluorescence image of HepG2 cells incubated with 10  $\mu$ M **2** for 30 min at 37  $^{\circ}$ C and then incubated with 10  $\mu$ M CuCl<sub>2</sub> for 30 min at 37  $^{\circ}$ C. (C) after (B), then incubated with Na<sub>2</sub>S (10  $\mu$ M) for 30 min at 37  $^{\circ}$ C. (D) after (B), then incubated with Na<sub>2</sub>S (20  $\mu$ M).

sensitivity toward  $\text{Cu}^{2+}$  that is comparable to the UV–vis probe **1** chemosensor.

### 3.9. Their application in anion biomaging

It is well known that chemosensor reversibility is required for reuse. Addition of  $\text{P}_2\text{O}_7^{4-}$  or  $\text{C}_2\text{O}_4^{2-}$  to the **1**- $\text{Cu}^{2+}$  complex in HEPES buffer (10 mmol/L, pH 7.0) results in the spectrum of **1** reverting to that of its original pre-complex state. Furthermore, when the concentrations of  $\text{P}_2\text{O}_7^{4-}$  or  $\text{C}_2\text{O}_4^{2-}$  are increased, the spectra renew gradually the spectra of free **1**. Simultaneously, the solution changes color from orange yellow to a light shade of yellow. For **2**, in addition to  $\text{P}_2\text{O}_7^{4-}$  and  $\text{C}_2\text{O}_4^{2-}$ , Cys,  $\text{S}_2\text{O}_3^{2-}$ ,  $\text{S}^{2-}$ , and citrate can play a similar role to that described. However, the addition of  $\text{P}_2\text{O}_7^{4-}$  and  $\text{C}_2\text{O}_4^{2-}$  results in a partial release of **3** from its complex (Fig. S16). Anions with a physiological function, including  $\text{F}^-$ ,  $\text{Cl}^-$ ,  $\text{Br}^-$ ,  $\text{I}^-$ , acetate ( $\text{AcO}^-$ ),  $\text{SCN}^-$ ,  $\text{NO}_3^-$ ,  $\text{SO}_4^{2-}$ ,  $\text{CO}_3^{2-}$ ,  $\text{C}_2\text{O}_4^{2-}$ ,  $\text{PO}_4^{3-}$ , and  $\text{CN}^-$ , were also investigated but their effect on the UV–vis spectra was not as evident as for  $\text{P}_2\text{O}_7^{4-}/\text{C}_2\text{O}_4^{2-}$ . These results indicate that **2** is an optimal probe for  $\text{Cu}^{2+}$  because it is easily regenerated.

The **2**- $\text{Cu}^{2+}$  complex exhibits an anion-induced increase in fluorescence, which thus allows for the possibility of using it in bioimaging. The ability of **2**- $\text{Cu}^{2+}$  to react with anions in living cells was also evaluated. Under selective excitation at 405 nm, HepG2 cells showed green fluorescence after they were incubated with 20  $\mu\text{mol/L}$  of **2** for 30 min at 37 °C, and with 10  $\mu\text{mol/L}$  of  $\text{S}^{2-}$  (as a delegate) added for the final 30 min (Fig. 7C). HepG2 cells incubated with probe **2** for 30 min at 37 °C with 20  $\mu\text{mol/L}$  of  $\text{S}^{2-}$  added for the final 30 min showed stronger green fluorescence (Fig. 7D). These cell experiments show that **2** can permeate through cell membranes.

## 4. Conclusions

Three compounds, namely 5-nitrosalicylaldehyde fluorescein hydrazone (**1**), 5-diethylaminosalicylaldehyde fluorescein hydrazone (**2**), and di(5-diethylamino salicylaldehyde) hydrazide (**3**), were successfully synthesized and characterized. Their abilities to recognize copper were investigated using UV–vis and fluorescence spectroscopies. The results showed that the recognition processes for each of the probes have some differences despite their similar structure, with the conclusion that probe **2** is an optimal probe for  $\text{Cu}^{2+}$ . More importantly, the optical properties of the probes and their  $\text{Cu}^{2+}$ -addition products were studied using DFT calculations and the fluorescence quenching mechanism revealed. Application in bioimaging was illustrated and anions can induce **2**- $\text{Cu}^{2+}$  to show strong fluorescence in living cells. This work will therefore prove useful for the future design and application of copper chemosensors.

## Acknowledgments

The work was supported by the National Natural Science Foundation of China (Nos. 21072119, 21102086), the Shanxi Province Science Foundation for Youths (No. 2012021009-4), the Shanxi Province Foundation for Returnee (No. 2012-007), the Taiyuan Technology star special (No. 12024703), Program for the Top Young Academic Leaders of Higher Learning Institutions of Shanxi (TYAL), and the Shanxi Province Foundation for Selected Returnees (no. 2010). We also thank Institute of Chemistry, Chinese Academy of Sciences, Beijing and Prof Zongxiu Nie.

## Appendix A. Supplementary data

Supplementary data associated with this article can be found, in the online version, at <http://dx.doi.org/10.1016/j.snb.2012.12.043>.

## References

- [1] Y.H. Chan, J. Chen, J.D. Batteas, Visual detection of copper(II) based on the aggregation of gold nano-particles via click chemistry, *Analytical Chemistry* 82 (2010) 3671–3678.
- [2] B. Ding, Y. Si, X. Wang, J. Yu, L. Feng, G. Sun, Label-free ultrasensitive colorimetric detection of copper(II) ions utilizing polyaniline/polyamide-6 nano-fiber/net sensor strips, *Journal of Materials Chemistry* 21 (2011) 13345–13353.
- [3] J. Liang, M. Qin, R. Xu, X. Gao, Y. Shen, Q. Xu, Y. Cao, W. Wang, A genetically encoded copper(I) sensor based on engineered structural distortion of EGFP, *Chemical Communications* 48 (2012) 3890–3892.
- [4] M. Shellaiah, Y.C. Rajan, H.C. Lin, Synthesis of novel triarylamine-based dendrimers with  $\text{N}^4, \text{N}^6$ -dibutyl-1,3,5-triazine-4,6-diamine probe for electron/energy transfers in H-bonded donor–acceptor–donor triads and as efficient  $\text{Cu}^{2+}$  sensors, *Journal of Materials Chemistry* 22 (2012) 8976–8987.
- [5] Y.F. Lee, T.W. Deng, W.J. Chiu, T.Y. Wei, P. Roy, C.C. Huang, Visual detection of copper(II) ions in blood samples by controlling the leaching of protein-capped gold nanoparticles, *Analyst* 137 (2012) 1800–1806.
- [6] Z. Lin, F. Luo, T. Dong, L. Zheng, Y. Wang, Y. Chi, G. Chen, Recyclable fluorescent gold nanocluster membrane for visual sensing of copper(II) ion in aqueous solution, *Analyst* 137 (2012) 2394–2399.
- [7] M.J. Tamás, E. Martinoia, *Molecular Biology of Metal Homeostasis and Detoxification: From Microbes to Man*, vol. 509, Springer, Berlin, NY, 2006, pp. 1–37.
- [8] R. Martínez, F. Zapata, P. Molina, 2-Aza-1,3-butadiene derivatives featuring an anthracene or pyrene unit: highly selective colorimetric and fluorescent signaling of  $\text{Cu}^{2+}$  cation, *Organic Letters* 8 (2006) 3235–3238.
- [9] V. Chandrasekhar, S. Das, R. Yadav, S. Hossain, R. Parihar, G. Subramaniam, P. Sen, Novel chemosensor for the visual detection of copper (II) in aqueous solution at the ppm level, *Inorganic Chemistry* 51 (2012) 8664–8666.
- [10] F. Hou, J. Cheng, P. Xi, F. Chen, L. Huang, G. Xie, Y. Shi, H. Liu, D. Bai, Z. Zeng, Recognition of copper and hydrogen sulfide in vitro using a fluorescein derivative indicator, *Dalton Transactions* 41 (2012) 5799–5804.
- [11] Guidelines for Drinking-water Quality, third edition, Incorporating First and Second Addenda, vol. 1, Recommendations, World Health Organization, 2006.
- [12] R. Krämer, Fluorescent chemosensors for  $\text{Cu}^{2+}$  ions: fast, selective and highly sensitive, *Angewandte Chemie International Edition* 37 (1998) 772–773.
- [13] G.L. Millhauser, Copper binding in the prion protein, *Accounts of Chemical Research* 37 (2004) 79–85.
- [14] E. Gaggelli, H. Kozłowski, D. Valensin, G. Valensin, Copper homeostasis and neurodegenerative disorders (Alzheimer's, prion, and Parkinson's diseases and amyotrophic lateral sclerosis), *Chemical Reviews* 106 (2006) 1995–2044.
- [15] J. Penga, X. Qua, G. Weia, J. Lia, J. Qiao, The cutting of MWNTs using gamma radiation in the presence of dilute sulfuric acid, *Carbon* 42 (2004) 2741–2744.
- [16] K.N. Buck, J.R.M. Ross, A.R. Flegel, K.W. Bruland, A review of total dissolved copper and its chemical speciation in San Francisco Bay, *Environmental Research* 105 (2007) 5–19.
- [17] E. Ballesteros, D. Moreno, T. Gómez, T. Rodríguez, J. Rojo, M. García-Valverde, T. Torroba, A new selective chromogenic and turn-on fluorogenic probe for copper (II) in water–acetonitrile 1:1 solution, *Organic Letters* 11 (2009) 1269–1272.
- [18] J.A. Camargo, Á. Alonso, Ecological and toxicological effects of inorganic nitrogen pollution in aquatic ecosystems: a global assessment, *Environment International* 32 (2006) 831–849.
- [19] J.F. Zhang, Y. Zhou, J. Yoon, J.S. Kim, *Chemical Society Reviews* 40 (2011) 3416–3429.
- [20] R. Martínez-Mañez, F. Sancenón, Fluorogenic and chromogenic chemosensors and reagents for anions, *Chemical Reviews* 103 (2003) 4419–4476.
- [21] Z. Xu, S.K. Kim, J. Yoon, Revisit to imidazolium receptors for the recognition of anions: highlighted research during 2006–2009, *Chemical Society Reviews* 39 (2010) 1457–1466.
- [22] P.A. Gale, Anion receptor chemistry: highlights from 2008 and 2009, *Chemical Society Reviews* 39 (2010) 3746–3771.
- [23] Z. Xu, X. Chen, H.N. Kim, J. Yoon, Sensors for the optical detection of cyanide ion, *Chemical Society Reviews* 39 (2010) 127–137.
- [24] Q. Wang, Y. Xie, Y. Ding, X. Li, W. Zhu, Colorimetric fluoride sensors based on deprotonation of pyrrole–hemiquinone compounds, *Chemical Communications* 46 (2010) 3669–3671.
- [25] Y. Ding, Y. Xie, X. Li, J.P. Hill, W. Zhang, W. Zhu, Selective and sensitive “turn-on” fluorescent  $\text{Zn}^{2+}$  sensors based on di- and tripyrins with readily modulated emission wavelengths, *Chemical Communications* 47 (2011) 5431–5433.
- [26] Y.J. Jang, B.S. Moon, M.S. Park, B.G. Kang, J.Y. Kwon, J.S.J. Hong, Y.J. Yoon, K.D. Lee, J. Yoon, New cavand derivatives bearing four coumarin groups as fluorescent chemosensors for  $\text{Cu}^{2+}$  and recognition of dicarboxylates utilizing  $\text{Cu}^{2+}$  complex, *Tetrahedron Letters* 47 (2006) 2707–2710.
- [27] H.S. Jung, P.S. Kwon, J.W. Lee, J.I. Kim, C.S. Hong, J.W. Kim, S. Yan, J.Y. Lee, J.H. Lee, T. Joo, J.S. Kim, Coumarin-derived  $\text{Cu}^{2+}$ -selective fluorescence sensor: synthesis, mechanisms, and applications in living cells, *Journal of the American Chemical Society* 131 (2009) 2008–2012.
- [28] A. Helal, M.H.O. Rashid, C.H. Choi, H.S. Kim, Chromogenic and fluorogenic sensing of  $\text{Cu}^{2+}$  based on coumarin, *Tetrahedron* 67 (2011) 2794–2802.
- [29] A.P. de Silva, H.Q. Nimal Gunaratne, T. Gunnlaugsson, A.J.M. Huxley, C.P. McCoy, J.T. Rademacher, T.E. Rice, Signaling recognition events with fluorescent sensors and switches, *Chemical Reviews* 97 (1997) 1515–1566.
- [30] M. Zhao, X. Yang, S. He, L. Wang, A rhodamine-based chromogenic and fluorescent chemosensor for copper ion in aqueous media, *Sensors and Actuators B* 135 (2009) 625–631.

- [31] C. Yu, L. Chen, J. Zhang, J. Li, P. Liu, W. Wang, B. Yan, "Off-On" based fluorescent chemosensor for Cu<sup>2+</sup> in aqueous media and living cells, *Talanta* 85 (2011) 1627–1633.
- [32] Z. Hu, X. Wang, Y. Feng, L. Ding, H. Lu, Sulfonyl rhodamine hydrazide: a sensitive and selective chromogenic and fluorescent chemodosimeter for copper ion in aqueous media, *Dyes and Pigments* 88 (2011) 257–261.
- [33] M. Dong, T. Ma, A. Zhang, Y. Dong, Y. Wang, Y. Peng, colorimetric "off-on" chemosensors for Cu (II) based on rhodamine derivatives, *Dyes and Pigments* 87 (2010) 164–172.
- [34] X. Chen, M. Jou, H. Lee, S. Kou, J. Lim, S. Nam, S. Park, K. Kim, J. Yoon, New fluorescent and colorimetric chemosensors bearing rhodamine and binaphthyl groups for the detection of Cu<sup>2+</sup>, *Sensors and Actuators B* 137 (2009) 597–602.
- [35] Y. Zhou, F. Wang, Y. Kim, S. Kim, J. Yoon, Cu<sup>2+</sup>-selective ratiometric and "Off-On" sensor based on the rhodamine derivative bearing pyrene group, *Organic Letters* 11 (2009) 4442–4445.
- [36] L. Jiang, B. Zhang, J. Sun, G. Yin, T. Shang, L. Wang, R. Wang, Dual channel rhodamine based colorimetric fluorescent probe for Cu<sup>2+</sup> in living cells, *Chinese Journal of Inorganic Chemistry* 26 (2010) 1750–1755.
- [37] X. Qi, E.J. Jun, S.J. Kim, J.S.J. Hong, Y.J. Yoon, New BODIPY derivatives as OFF-ON fluorescent chemosensor and fluorescent chemodosimeter for Cu<sup>2+</sup>: cooperative selectivity enhancement toward Cu<sup>2+</sup>, *Journal of Organic Chemistry* 71 (2006) 2881–2884.
- [38] L. Zeng, E.W. Miller, A. Pralle, E.Y. Isacoff, C.J. Chang, A selective turn-on fluorescent sensor for imaging copper in living cells, *Journal of the American Chemical Society* 128 (2006) 10–11.
- [39] K. Rurack, M. Kollmannsberger, U. Resch-Genger, J. Daub, A selective and sensitive fluoroionophore for HgII, AgI, and CuI with virtually decoupled fluorophore and receptor units, *Journal of the American Chemical Society* 122 (2000) 968–969.
- [40] C.Y. Li, Q.Y. Zheng, C.F. Chen, Z.T. Huang, Fluorescent probes of D calix[5] arene, *Tetrahedron: Asymmetry* 16 (2005) 2816–2820.
- [41] Z. Liang, Z. Liu, L. Jiang, Y. Gao, A new fluorescent chemosensor for copper(II) and molecular switch controlled by light, *Tetrahedron Letters* 48 (2007) 1629–1632.
- [42] V. Bhalla, R. Kumar, M. Kumar, A. Dhir, Bifunctional fluorescent thiacalix[4]arene based chemosensor for Cu<sup>2+</sup> and F<sup>-</sup> ions, *Tetrahedron* 59 (2003) 3267–3273.
- [43] N. Singh, M. Kumar, G. Hundal, Synthesis, NMR, X-ray structural analyses and complexation studies of new Ag<sup>+</sup> selective calix[4]arene based dipodal hosts – a co-complexation of neutral and charged species, *Tetrahedron* 60 (2004) 5393–5405.
- [44] A.K. Mahapatra, G. Hazra, N.K. Das, S. Goswami, A highly selective triphenylamine-based indolylmethane derivatives as colorimetric and turn-off fluorimetric sensor toward Cu<sup>2+</sup> detection by deprotonation of secondary amines, *Sensors and Actuators B* 156 (2011) 456–462.
- [45] A. Helal, S.H. Lee, S.H. Kim, H.S. Kim, Dual-signaling fluorescent chemosensor based on bisthiazole derivatives, *Tetrahedron Letters* 51 (2010) 3531–3535.
- [46] R. Martínez, A. Espinosa, A. Tárraga, P. Molina, Bis(indolyl)methane derivatives as highly selective colorimetric and ratiometric fluorescent molecular chemosensors for Cu<sup>2+</sup> cations, *Tetrahedron* 64 (2008) 2184–2191.
- [47] F.J. Huo, J. Su, Y.Q. Sun, C.X. Yin, H.B. Tong, Z.X. Nie, A rhodamine-based dual chemosensor for the visual detection of copper and the ratiometric fluorescent detection of vanadium, *Dyes and Pigments* 86 (2010) 50–55.
- [48] F.J. Huo, C.X. Yin, Y.T. Yang, J. Su, J.B. Chao, D.S. Liu, Ultraviolet-visible light (UV-vis)-reversible but fluorescence-irreversible chemosensor for copper in water and its application in living cells, *Analytical Chemistry* 84 (2012) 2219–2223.
- [49] G.M. Sheldrick, SADABS, University of Göttingen, Germany, 1997.
- [50] G.M. Sheldrick, Program for the Refinement of Crystal Structure, University of Göttingen, Germany, 1997.
- [51] X.F. Yang, D.B. Wu, H. Li, 2'-Amino-3,6-dihydroxy xanthene-9-spiro-1'-isoindolin-3'-one monohydrate, *Microchimica Acta* 149 (2005) 123–129.
- [52] F.A. Abebe, C.S. Eribal, G. Ramakrishna, E. Sinn, Department of A 'turn-on' fluorescent sensor for the selective detection of cobalt and nickel ions in aqueous media, *Tetrahedron Letters* 52 (2011) 5554–5558.
- [53] L.M. Hyman, C.J. Stephenson, M.G. Dickens, K.D. Shimizu, K.J. Franz, Toward the development of prochelators as fluorescent probes of copper-mediated oxidative stress, *Dalton Transactions* 39 (2010) 568–576.
- [54] X. Chen, Z. Li, Y. Xiang, A. Tong, *Tetrahedron Letters* 49 (2008) 4697–4700.
- [55] K.M.K. Swamy, S. Ko, S.K. Kwon, H. Lee, C. Mao, J. Kim, K. Lee, J. Kim, I. Shin, J. Yoon, Salicylaldehyde fluorescein hydrazone: a colorimetric logic chemosensor for pH and Cu(II) boronic acid-linked fluorescent and colorimetric probes for copper ions, *Chemical Communications* (2008) 5915–5917.
- [56] Y. Xiang, Z. Li, X. Chen, A. Tong, Highly sensitive and selective optical chemosensor for determination of Cu<sup>2+</sup> in aqueous solution, *Talanta* 74 (2008) 1148–1153.
- [57] M. Salavati-Niasari, A. Amiri, Synthesis and characterization of alumina-supported Mn(II), Co(II), Ni(II) and Cu(II) complexes of bis(salicylaldehyde)hydrazone as catalysts for oxidation of cyclohexene with tert-butylhydroperoxide, *Applied Catalysis A: General* 290 (2005) 46–53.
- [58] H.S. Jung, K.C. Ko, G.H. Kim, A.R. Lee, Y.C. Na, C. Kang, J.Y. Lee, J.S. Kim, Coumarin-based thiol chemosensor: synthesis, turn-on mechanism, and its biological application, *Organic Letters* 13 (2011) 1498–1501.
- [59] Q. Li, M. Peng, H. Li, C. Zhong, L. Zhang, X. Cheng, X. Peng, Q. Wang, J. Qin, Z. Li, A new "turn-on" naphthalenedimide-based chemosensor for mercury ions with high selectivity: successful utilization of the mechanism of twisted intramolecular charge transfer, near-IR fluorescence, and cell images, *Organic Letters* 14 (2012) 2094–2097.
- [60] L. Deng, W. Wu, H. Guo, J. Zhao, S. Ji, X. Zhang, X. Yuan, C. Zhang, Colorimetric and ratiometric fluorescent chemosensor based on diketopyrrolopyrrole (DPP) for selective detection of thiols: an experimental and theoretical study, *Journal of Organic Chemistry* 76 (2011) 9294–9304.

## Biographies

**Yutao Yang** is studying for the doctorate program in Institute of Molecular Science at Shanxi University. She received her BSc in chemistry for Shanxi University in 2008.

**Fangjun Huo** is an Associate Professor in Research Institute of Applied Chemistry at Shanxi University major in organic chemistry. His current research interests are sensors and supramolecular chemistry.

**Caixia Yin** is a Professor in Key Laboratory of Chemical Biology and Molecular Engineering of Ministry of Education, Institute of Molecular Science at Shanxi University, and has majored in inorganic chemistry. Her current research interests are molecular recognition and sensors chemistry.

**Yueyin Chu** is studying for Masters degree in Wuhan Institute of Physics and Mathematics, the Chinese Academy of Sciences. She received her BSc degree in chemistry from the chemistry department of Central China normal university in 2008.

**Jianbin Chao** is an Associate Professor in Research Institute of Applied Chemistry at Shanxi University major in organic chemistry. His current research interests are supramolecular chemistry.

**Yongbin Zhang** is an Associate Professor in Research Institute of Applied Chemistry at Shanxi University and has majored in organic chemistry. His current research interests are synthesis chemistry.

**Jingjing Zhang** is studying for masters degree in Institute of Molecular Science at Shanxi University. She received his BSc degree in chemistry from Yuncheng University in 2010.

**Sidiang Li** is a Professor in Key Laboratory of Chemical Biology and Molecular Engineering of Ministry of Education, Institute of Molecular Science at Shanxi University and has majored in inorganic chemistry. His current research interests are material chemistry and calculation chemistry.

**Haigang Lv** is a lecturer in Key Laboratory of Chemical Biology and Molecular Engineering of Ministry of Education, Institute of Molecular Science at Shanxi University and has majored in inorganic chemistry. His current research interest is calculation chemistry.

**AnminZheng** is an Associate Professor in Wuhan Institute of Physics and Mathematics, the Chinese Academy of Sciences and has majored in physical chemistry. His current research interest is calculation chemistry.

**Diansheng Liu** is a Professor in Research Institute of Applied Chemistry at Shanxi University and has majored in organic chemistry. His current research interest is synthesis chemistry.